Cryo-electron tomography of mouse hepatitis virus: Insights into the structure of the coronavirion

Montserrat Bárcena[a], Gert T. Oostergetel[b], Willem Bartelink[c], Frank G. A. Faas[a], Arie Verkleij[d], Peter J. M. Rottier[c], Abraham J. Koster[a,1], and Berend Jan Bosch[c]

[a]Department of Molecular Cell Biology, Electron Microscopy Section, Leiden University Medical Center, 2300 RC, Leiden, The Netherlands; [b]Biophysical Chemistry, Groningen Biomolecular Sciences and Biotechnology Institute, University of Groningen, 9497 AG, Groningen, The Netherlands; [c]Department of Infectious Diseases and Immunology, Virology Division, Faculty of Veterinary Medicine, Utrecht University, 3584 CL, Utrecht, The Netherlands; and [d]Department of Molecular Cell Biology, Utrecht University, 3584 CH, Utrecht, The Netherlands

Edited by Stanley Perlman, University of Iowa, Iowa City, IA, and accepted by the Editorial Board November 20, 2008 (received for review June 3, 2008)

Coronaviruses are enveloped viruses containing the largest reported RNA genomes. As a result of their pleomorphic nature, our structural insight into the coronavirion is still rudimentary, and it is based mainly on 2D electron microscopy. Here we report the 3D virion structure of coronaviruses obtained by cryo-electron tomography. Our study focused primarily on the coronavirus prototype murine hepatitis virus (MHV). MHV particles have a distinctly spherical shape and a relatively homogenous size (≈85 nm envelope diameter). The viral envelope exhibits an unusual thickness (7.8 ± 0.7 nm), almost twice that of a typical biological membrane. Focal pairs revealed the existence of an extra internal layer, most likely formed by the C-terminal domains of the major envelope protein M. In the interior of the particles, coiled structures and tubular shapes are observed, consistent with a helical nucleocapsid model. Our reconstructions provide no evidence of a shelled core. Instead, the ribonucleoprotein seems to be extensively folded onto itself, assuming a compact structure that tends to closely follow the envelope at a distance of ≈4 nm. Focal contact points and thread-like densities connecting the envelope and the ribonucleoprotein are revealed in the tomograms. Transmissible gastroenteritis coronavirion tomograms confirm all the general features and global architecture observed for MHV. We propose a general model for the structure of the coronavirion in which our own and published observations are combined.

coronaviruses | enveloped viruses | plus-stranded RNA viruses | transmissible gastroenteritis coronavirus

Coronaviruses (CoVs) are large, enveloped, plus-stranded RNA viruses that infect a wide variety of avians and mammals. Several CoVs are human pathogens, including the causative agent of severe acute respiratory syndrome (SARS) (1, 2). The SARS outbreak in 2002–2003 served as a grim reminder of these viruses' potential to cross the species barrier and triggered a renewed interest in CoVs. Since then, new CoVs have come to expand the list of discovered members, with two more respiratory human CoVs among them (3, 4).

The current virion model of CoVs, based on morphological and biochemical data, depicts a pleomorphic particle that is roughly spherical but shows variations in size (80–120 nm) and shape (reviewed in refs. 5, 6). The virion contains the ribonucleoprotein (RNP) core, consisting of a genomic RNA that is the largest among all RNA viruses (≈30 kb), in complex with the nucleocapsid (N) protein (≈380–450 aa). The RNP is surrounded by a lipidic envelope. Three viral proteins are anchored in the envelope of all CoVs: the abundant triple-spanning membrane (M) protein (≈230 aa), the envelope (E) protein (≈100 aa; present in only small amounts), and the spike (S) protein (≈1,300 aa), forming trimeric spikes. The spikes are responsible for receptor binding and membrane fusion and extend radially from the envelope, giving the virions a solar image to which coronaviruses owe their name. The M protein appears to be the building brick of the virion and is thought to orchestrate virion assembly via interactions with all viral components, including itself. Virus-like particles devoid of RNP and S can be formed upon co-expression of M and E (7).

Despite multiple biochemical and morphological studies, many fundamental aspects of the virion architecture remain to be elucidated. The structure of the coronavirus RNP core has been particularly elusive. In negatively stained intact virions, the interior is not visible, and thus early studies focused on samples in which the viral envelope was disrupted and the inner content released. RNPs extracted in this way from several CoVs appear to have helical symmetry (8–10). However, under certain conditions, intermediate spherical nucleocapsids have been reported (11, 12). These structures, which showed polygonal profiles, were devoid of S protein and lipids but, in addition to RNA and the N protein, contained the M protein (12). These assemblies were suggested to represent an additional viral structure: a shelled core, possibly even icosahedral, that would enclose the helical RNP (12). In cryo-electron microscopy, in which the contrast arises from the specimen itself, the internal content becomes apparent in undisrupted viruses (12–14). However, the superposition of viral features in projection images hampers their structural interpretation.

To a large extent, the pleomorphic nature of CoVs has been the main obstacle to clarifying details of their structure, as the particles are not identical and therefore cannot be analyzed by single particle averaging methods (15). To overcome this limitation, we have studied murine hepatitis virus (MHV; CoV group 2), the prototypic CoV, by cryo-electron tomography and have obtained 3D reconstructions of CoVs. The 3D nature of the data was particularly useful to gain insight into the inner structure of the intact virus. As cyro-electron tomography provides a 3D structure for each individual virus particle in the sample, our results show the morphological variations within the viral population together with common structural motifs. Cryo-tomography of transmissible gastroenteritis coronavirus (TGEV; CoV group 1) reveals a similar virion organization, suggesting a general model for the architecture of CoVs.

Results

Cryo-Electron Tomography of MHV. Purified MHV samples were rapidly cryo-fixed by plunge freezing. A total of 7 tilt series were collected at a relatively low defocus (4 μm) to preserve fine

Author contributions: M.B., P.J.M.R., A.J.K., and B.J.B. designed research; M.B., G.T.O., W.B., and B.J.B. performed research; G.T.O., F.G.A.F., and A.V. contributed new reagents/analytic tools; M.B., F.G.A.F., A.J.K., and B.J.B. analyzed data; and M.B. wrote the paper.

The authors declare no conflict of interest.

This article is a PNAS Direct Submission. S.P. is a guest editor invited by the Editorial Board.

Freely available online through the PNAS open access option.

[1]To whom correspondence should be addressed. E-mail: a.j.koster@lumc.nl.

This article contains supporting information online at www.pnas.org/cgi/content/full/0805270106/DCSupplemental.

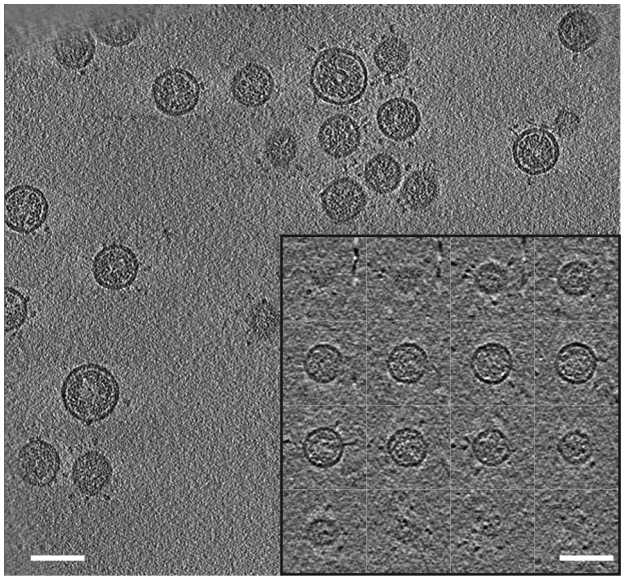

Fig. 1. Virtual slice (8.7 nm thick) in one of the reconstructed fields of purified MHV particles. *Inset*, Z-slices (5.8 nm thick) through one of the MHV cryo-tomograms. (Scale bars, 100 nm.)

detail contrast transfer. Fig. 1 shows one of the reconstructed areas, illustrating the typical distribution and general preservation of the particles in the preparations (see also Movie S1 and Movie S2). Three-dimensional density maps of 144 virions were computed from these data sets.

General Features of MHV. The shape of the reconstructed MHVs appeared to be remarkably homogeneous. The large majority of the virions exhibit a distinct spherical form (Fig. 1). This is in contrast not only with early studies of negatively stained CoVs, in which distortions were known to account for part of the heterogeneity observed, but also with previous cryo-electron microscopy images in which CoVs appear elliptical (14). Only ≈7% of the MHVs in our samples showed ellipticity; however, our data strongly suggest this to be a result of distortions induced in the proximity of the water-air interface (Fig. S1). Therefore, the subsequent analysis focused on the remaining 135 spherical virions.

The size range of MHV particles is shown in Fig. 2. The variation in envelope size follows a smooth distribution around a mean value of 85 ± 5 nm (SD) in diameter (n = 131), except for some rare, clearly larger MHVs (diameter ≈103 nm, n = 4), which seem to constitute an independent class. Examples of

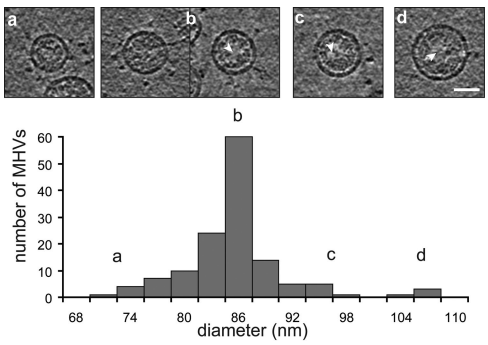

Fig. 2. Size histogram of MHV particles. Central sections (5.8 nm thick) of virions from the different regions of the histogram are shown in *A–D*. The arrows point at lower-density areas inside the virion. (Scale bar, 50 nm.)

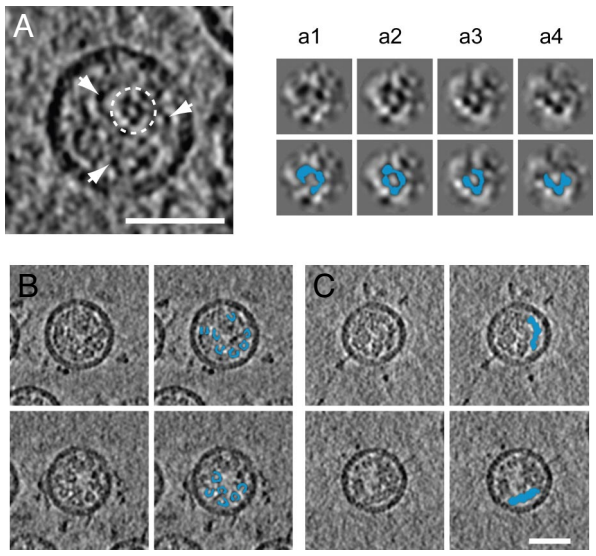

Fig. 3. (*A*) Slice through one of the reconstructed MHV particles (5.8 nm thick). The arrows point to some of the granular densities visible in the virion interior. These are likely to correspond to the N protein in complex with RNA. The dashed circle encloses a quasi-circular profile formed by these densities. (*A*). Serial sections (4 nm thick) of this region encompassing a total height of 11 nm. (*B* and *C*) Thick virtual slices (11 nm thick) of four different MHV particles displaying (*B*) circular profiles and (*C*) tubular fragments. These patterns are colored in blue. Assuming that they are favorable orientations of the RNP coil, a number of 4 to 5 granular densities per turn and a pitch of ≈10 nm were estimated. (Scale bars, 50 nm.)

differently sized MHV particles found in our preparations are shown in the gallery of Fig. 2. The viruses share a similar appearance and a detailed analysis did not reveal size-dependent differences in any of the viral features discussed in the next sections.

Ribonucleoprotein Complex. Our reconstructions show the interior of MHV particles to be filled with material. In some instances, however, a central region of lower density was observed (see Fig. 2). Although these areas are more common in larger particles, their presence and extent are not systematically correlated with the virion size. Except for these lower-density regions, the RNP seems to be relatively densely packed and disorganized underneath the envelope. In thin virtual sections, the interior of the virion appears to contain distinct granular densities (Fig. 3*A*). After careful examination of the complex density network, certain regular patterns become apparent. One of the most prominent characteristics is the presence, in an otherwise relatively disorganized interior, of quasi-circular density profiles approximately 11 nm in diameter enclosing an empty space approximately 4 nm in diameter.

Previous studies of negatively stained RNP complexes extracted from disrupted CoVs revealed thread-like coil structures with diameters of 9 to 16 nm and a hollow interior of approximately 3 to 4 nm (9, 10). Given the similarity in dimensions and appearance, we interpret the quasi-circular profiles observed in the 3D maps as turns of the coiled RNP when viewed close to the direction along to the coil axis. In agreement with this interpretation, the quasi-circular profiles rotate along consecutive sections, indicating their nature as part of coiled structures (Fig. 3*A*). In thicker virtual slices, in which the noise is reduced, this pattern becomes more apparent (Fig. 3*B*). Moreover, tubular shapes can be distinguished (Fig. 3*C*), suggesting that they correspond to favorable cases in which stretches of the coiled structure lie almost parallel to the XY plane.

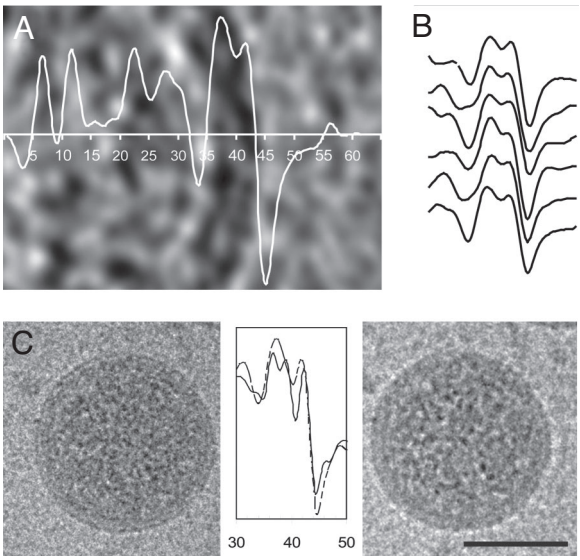

Fig. 4. MHV envelope. (*A*) Radial density profile of the rotationally averaged image superimposed to a central slice of the virion (5.8 nm thick). (*B*) Several density profiles of the envelope of reconstructed MHV particles. (*C*) Focal pairs of an MHV particle at 2 μm (*Left*) and 4 μm underfocus (*Right*), and radial density profiles (continuous line, 2 μm underfocus; dashed line, 4 μm underfocus). All measurements are in nanometers. (Scale bars, 50 nm.)

After several slices, the circular profiles quickly turn into different shapes, which would be consistent with a flexible coiled structure folding back onto itself. However, such an entangled internal arrangement, combined with the lower resolution in the Z direction inherent to electron tomography data, hinder a straightforward interpretation of many of the densities observed and the tracing of the continuous RNP structure.

Viral Envelope. The first striking feature of the MHV envelope in the reconstructions was its exceptional thickness, approximately 7 to 8 nm as measured directly on XY sections. For a more quantitative analysis, an automatic procedure based on the rotationally averaged density profiles was used (see *SI Text*), yielding a value of 7.8 nm (SD = 0.7, n = 58). This value largely exceeds the average thickness of biological membranes, which is ≈4 nm (16). A second interesting finding was the bilaminar appearance of the envelope, reflected in two peaks in the density profiles (Fig. 4 *A* and *B*).

At the relatively large underfocus value (4 μm) used for cryo-tomography, modifications of the images by the contrast transfer function of the microscope are expected. Therefore, to properly interpret these observations, we collected focal pairs of MHV and, for comparison with a pure lipid bilayer, of DOPC (1,2-dioleoyl-sn-glycero-3-phosphocholine) liposomes (see *SI Text* and Fig. S2). The analysis of these images showed that, in the defocus range examined (1, 2, 4, and 8 μm), the apparent thickness of the envelope does not change. The value for the MHV envelope thickness was confirmed (7.6 ± 0.4 nm, n = 101) and shown to be clearly larger than that of the DOPC lipid bilayers (4.2 ± 0.7 nm, n = 81). Furthermore, the inner peak of the bilaminar profile at 4 μm underfocus resolves in two at ≤2 μm underfocus (Fig. 4*C*).

This indicates the existence of an additional layer that would confer the virion envelope its remarkable thickness. We propose the inner lamina to be formed by the C-terminal domain of the M protein. Only a major component of the envelope, such as the M protein, could account for this general envelope feature. A topological model for the M protein of MHV has been proposed based on its hydrophobicity profile and on biochemical data

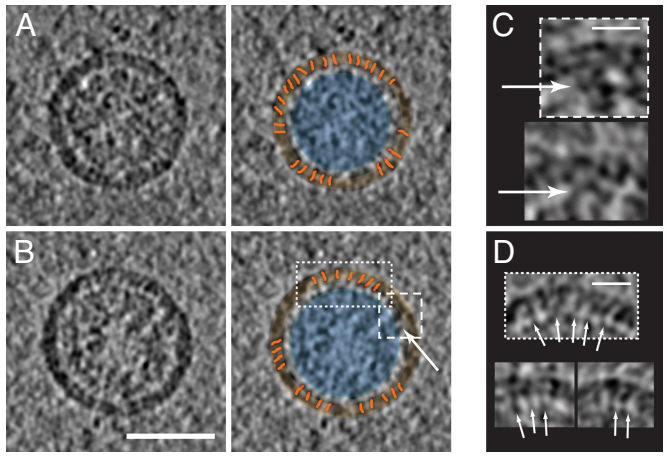

Fig. 5. (*A* and *B*) Two 7.5-nm sections through two different MHV particles (*Left*) and highlighted features superimposed (*Right*). The striations in the envelope have been colored in orange. The RNP region is colored in blue and the envelope in orange to highlight the ≈4-nm low-density region in between. The arrow points to one of the focal contact points. (Scale bar, 50 nm.) (*C* and *D*) Close-ups of the focal contact points (*C*) and linking densities (*D*) between the RNP and envelope, indicated by arrows. The framed images are enlargements of the corresponding boxed areas in *B*. (Scale bar, 15 nm.)

(17–19). The protein consists of 3 transmembrane domains contained within its amino-terminal half, followed by a carboxy-terminal domain that is assumed to be located toward the interior of the virus. The carboxy-domain by itself has been found to associate with membranes (20), and most of it is resistant to protease treatment (18), indicating that this part is folded tightly onto the polar surface of the membrane. Assuming a globular conformation for the 9.5-kDa C-terminal domain, and a protein partial specific volume of 0.75 g/cm^3, its diameter would be 2.8 nm. This is in good agreement with the thickness of the observed internal layer, which we estimate to be ≈3 nm based on the distance between peaks.

Another conspicuous feature of the envelope's ultrastructure is the existence of striations, which we also attribute to the M protein. In XY sections, these transversal densities were often separated by a relatively regular distance (Fig. 5), suggesting local order. A deeper analysis in 3D showed that the striation distribution was different from random, with a preferred neighbor distance of ≈6.5 nm, independent of the virus size (Fig. S3).

Interactions between the M protein with the genomic RNA and the N protein are thought to be the driving force for packaging CoV genomes into new virions (21–23). Focal contact points between the RNP and the envelope were observed in the tomograms (Fig. 5*B*). Additionally, we detected hints of thin, thread-like connections between the striations in the envelope and the inner mass of the virion (Fig. 5*C*).

In a recent 2D cryo-microscopy study, it has been proposed that the RNP could be forming a lattice underlying the envelope (14). We do not find direct evidence of such a structure in our data, although the resolution limitations of cryo-tomography would make such a lattice very hard to detect. In any case, the infoldings and extensions of the RNP in the reconstructions suggest that, if ordered arrangements exist, they would be local.

Spikes. The MHV spikes found in our tomograms have an average length of ≈20 ± 2 nm (n = 50) and show the typical club-like shape consisting of a stalk plus a roughly globular head of approximately the same length each (≈10 ± 2 nm). None of the virus particles in our reconstructions showed a continuous corona of spikes. The average number of spikes per virion was 10.8, which would correspond to ≈15% coverage, assuming a

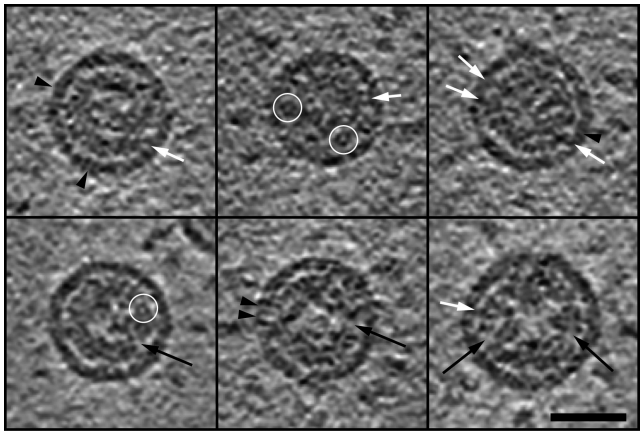

Fig. 6. Gallery of central virtual slices through some of the reconstructed TGEV particles (5.8 nm thick). TGEV virions show the same global architecture as MHV and analogous structural details (some of which are indicated). The RNP forms a complex arrangement with granular appearance in which some quasi-circular profiles (encircled in white) can be distinguished. The RNP closely follows the membrane at a distance of ≈4 nm, although infoldings (black arrows) and extensions contacting the envelope (white arrows) can be observed. Striations (black arrowheads) are visible in the TGEV virion envelope. (Scale bar, 50 nm.)

similar spike spacing as for SARS-CoV (13). Patches of only 4 to 8 spikes were detected, and isolated spikes were the most common finding. A similar incomplete spike coverage was observed in images of viruses that were taken from the medium directly, or from medium after paraformaldehyde fixation (data not shown). Therefore, this seems to be an intrinsic characteristic of our preparations. The situation resembles that of HIV, which has been shown to posses quite a limited number of spikes in cryo-tomograms (24).

The CoV spike proteins are dispensable for virus assembly (25, 26), although they are essential for infection. However, the number of peplomers actually required for an infection event might be relatively low. Biochemical data indicate that as few as one spike could be sufficient in the case of HIV (27). Although no equivalent information is available for CoVs, the infectivity of the virion preparations analyzed here suggests that only a limited number of spikes could be sufficient to trigger infection.

Cryo-Electron Tomography of TGEV. To investigate the generality of our observations on MHV, a limited cryo-tomography study was also carried out with TGEV. Four tilt series were collected at the same defocus as for MHV tomography (4 μm). A total of 56 TGEV particles were extracted from these series and independently reconstructed and analyzed.

TGEV virions in the tomograms show a typical spherical shape (Fig. 6 and Movie S3) and an average envelope diameter of 81 ± 5 nm with sizes ranging from 65 to 93 nm. As in the case of MHV, a minor proportion of larger virions (diameter >100 nm) was observed. Interestingly, large TGEV particles have been detected before and were proposed to be intracellular precursors of the small virions, although ≈1% to 5% seemed to escape this putative maturation process and were secreted (28, 29). The large TGEV and MHV particles observed in our preparations could represent such a class.

Some reconstructed TGEVs are shown in Fig. 6. TGEV cryo-tomograms revealed a global virion architecture analogous to that of MHV. Thus, the RNP inside the virion forms a complex and compact arrangement that is separated by the envelope by a relatively constant distance of ≈4 nm, although infoldings and extensions are observed throughout the sections. The tomograms show no indication of an additional shelled structure. Contact points between the internal RNP and the envelope are apparent in the tomograms.

As in the case of MHV, the TGEV viral envelope was shown to be almost twice as thick as a lipid bilayer (7.4 ± 0.6 nm), and exhibited a bilaminar appearance in the tomograms and in the corresponding density profiles (not shown). A 2D focal-pair analysis of cryo-images showed that the TGEV envelope resolves in a trilaminar profile at an underfocus value of 2 μm (see Fig. S2), consistent with the MHV results.

Although TGEV particles in our preparations possessed a larger number of spikes than MHV, the coverage also showed to be incomplete (average coverage ≈50% ± 15%). TGEV spikes are similar in size and shape to MHV peplomers. They have an average length of ≈21 ± 2 nm (n = 50), and consist of a stalk (≈10 ± 2 nm) and a globular head (≈11 ± 2 nm) that confers them the typical club-like shape of coronavirus spikes.

Discussion

Our understanding of the ultrastructure of large enveloped viruses, such as CoVs, has been hampered by the variations in size and shape they quite often exhibit. Cryo-electron tomography is starting to shed light onto the 3D structure of this type of viruses, whose pleomorphic nature denotes a structural plasticity that may well play an essential role in the virus life cycle (30). Our cryo-tomograms of whole coronavirions provide direct insight into the 3D structure of CoVs, revealing important features of the virion envelope and the RNP.

The envelope of our reconstructed MHV particles exhibits an unusual thickness of 7.8 ± 0.7 nm (7.4 ± 0.6 nm for TGEV). This almost doubles the ≈4 nm value known for average biological membranes (16), as well as the 4.2 ± 0.7 nm thickness we measured for pure lipid bilayers in DOPC liposomes. In the tomograms, two layers can be distinguished in the envelope. Interestingly, the inner layer resolves into two in lower defocus images, revealing an extra concentric shell in addition to the lipid bilayer. We propose that this extra layer represents the C-terminal domain of the M protein arranged in close apposition to the inner leaflet of the lipid bilayer (20). This domain is known to fold compactly (19) and to associate with membranes when expressed by itself. Here it should be noted that an alternative topology in which the C-terminal domain would be at the outside of the virion has been found for the M protein of TGEV, although only in a minor proportion (31).

The observed organization of the CoV envelope is reminiscent of that of the many RNA viruses that contain a matrix protein, which forms a distinct layer underneath the viral membrane as it is, for instance, shown in cryo-EM images of influenza virus (32, 33) and immature retrovirus particles (34–36). However, in contrast to conventional matrix proteins, the C-terminal matrix domain of the coronavirus M protein is unique in being an integral part of an envelope protein.

Matrix proteins connect the virion envelope and the viral core, which is consistent with the function of the M protein. The M protein not only interacts with all membrane components, thereby facilitating their incorporation into the virion (5), but it also connects to both components of the RNP—the N protein and the RNA genome—thus mediating RNP packaging. The interaction with the RNP occurs via its ≈25-aa-long hydrophilic C-terminal tail (21, 37). In our tomograms we find indirect and direct evidence of these interactions. The RNP structure closely follows the membrane, from which it is separated by a gap of approximately 4 nm. This regular spacing should reflect interplay between both structural components. Furthermore, we have directly visualized (*i*) regions of close contact and (*ii*) fine thread-like connections between the envelope and the RNP. Both are likely to represent interaction sites. In EM images of infected cells, curved membrane profiles have been observed at the site of budding in the endoplasmic reticulum and endoplas-

mic reticulum-Golgi intermediate compartment (28), where the RNP is recruited via interactions with the M protein. The matrix-like organization of the M protein underneath the membrane most likely provides an assembly scaffold for the RNP to be packaged into the virion.

Our analysis of the viral envelope further reveals the presence of striations, most likely attributable to the M protein. Analysis in 3D for MHV showed that, although a clear striation lattice (e.g., hexagonal) was not apparent in the data, there is a preferred neighbor distance of ≈6.5 nm. This suggests M protein organization at a local level. M proteins have been shown to establish multiple homotypical interactions that are considered to play a key role in viral morphogenesis (38–40), and which could account for our observation. It is even possible that the striations themselves represent higher oligomeric states of the M protein, although resolution limitations do not allow us to directly establish this point. However, considering that the M protein C-terminal domain would have a predicted size of ≈2.8 nm if globular and based on sterical constraints, the intra-striation distance of ≈6.5 nm suggests an upper limit of an M tetramer per striation.

In our 3D reconstructions, the interior of the coronavirions appears to be organized quite compactly in a quasi-globular arrangement that lacks detectable icosahedral symmetry but in which infoldings and extensions are systematically observed in successive XY slices. These discontinuities, which would not be resolved in projection images because of the overlap of features, contradict the notion of a proteinaceous enclosing shell, as proposed before (12). The latter interpretation was mainly based on images of the released content of disrupted virions, leaving open the question whether the observed structures faithfully represent the content of the virus or a rearrangement of structural elements resulting from the treatment. With cryo-tomography, we could overcome these difficulties and examine the intact content of the virions in situ.

Despite the complexity of the inner content manifested in the tomograms, regularly sized patterns of approximately 11 nm including quasi-circular profiles and tubular-like fragments are apparent in the MHV reconstructions. These patterns are consistent with the model of a helical arrangement of the RNP. Actually, we could directly detect coils in cases in which their orientation was favorable, with the coil axis perpendicular to the XY plane. Helical cores are exceptional among positive-stranded RNA viruses, in which icosahedral capsids are the most usual arrangement. In this respect, CoVs would be more similar to negative-stranded RNA viruses, in which the norm seems to be a helical core. Actually, the interior of MHV as revealed in this study shows a remarkable analogy with that of influenza A virions. A similar loose arrangement of coiled structures was detected for this most abundant group of the orthomyxoviruses (33). Yet, these viruses are different in many respects. Whereas orthomyxoviruses have segmented RNA genomes, the CoV genome is a non-segmented RNA of ≈30 kb. The coils that we observe are thus part of a continuous structure formed by self-association of the N protein and the genomic RNA. The fact that only short coiled fragments are detectable in the reconstructions strongly suggests that the helical nucleocapsid is a very flexible structure that extensively twists and folds upon itself, rapidly adopting orientations that would not be recognizable as coils in tomographic sections. The presence of less organized RNP regions, which might additionally help to fold the RNP coil structure, cannot be discarded. This flexibility might be the key to allow CoVs to package a genomic RNA that is the largest among all RNA viruses.

On the basis of our observations, we propose a new model for the CoV structure (Fig. 7). The model envisages an infectious virus particle not necessarily fully covered with spikes, which is limited by a proteolipid envelope in which the M protein takes a prominent position, and that contains a flexible RNP core that is at least partially helical. The global picture that emerges from our reconstructions is that of a virion whose general architecture is based upon several ordered structural elements (helical fragments, local order of the M protein, RNP-envelope interaction points), which may alternate with less organized regions. This type of arrangement would possess the adaptability needed to reproduce the same architecture in virions of different sizes by providing the modules that would serve as the basic framework for the virion structure.

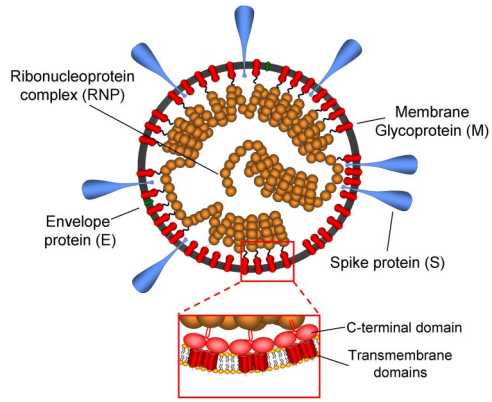

Fig. 7. Structural model of the coronavirion based on our interpretation of the tomograms. Segments of unordered RNP alternate with coils in the interior of the virion. M monomers, dimers, trimers, and/or tetramers distribute all over the envelope and interact with each other at a local level. The C-terminal domains of the M proteins constitute an extra layer coating the interior of the lipid membrane (*Inset*). The focal contacts and string connections between the envelope and the RNP suggest anchor points for virion assembly and integrity.

Materials and Methods

Virus Purification. LR7 and PD5 cells were maintained as monolayer cultures in Dulbecco modified Eagle medium (DMEM) supplemented with 10% FCS (Bodinco), 100 IU of penicillin/mL, and 100 μg of streptomycin/mL (P/S; Life Technologies).

LR7 cells were inoculated with MHV (strain A59) in DMEM at a multiplicity of infection of 5. At 1 h after infection, cells were washed with medium and the medium replaced by DMEM containing FCS, P/S, and 1 μM HR2 peptide to prevent syncytia formation (41). At 15 h after infection, the culture medium was harvested and centrifuged for 10 min at 3,000 rpm at 4°C to remove cellular debris. Virions in the supernatant were sedimented through a 20% sucrose cushion (wt/wt) in MM buffer [20 mM 2-(N-morpholino)ethanesulfonic acid (Mes), pH 6.0, 20 mM $MgCl_2$] by ultra-centrifugation at 20,000 rpm for 1.5 h at 4°C in a Beckman SW28 rotor.

PD5 cells were inoculated with TGEV (strain Purdue) in PBS-Ca/Mg plus 50 mg/L DEAE-dextran at a multiplicity of infection of 0.1. At 1 h after infection, inoculum was replaced by DMEM containing 5% FCS and P/S. At 20 h after infection, the culture medium was harvested and centrifuged for 10 min at 7,500 rpm at 4°C in a Beckman SW32 Ti rotor to remove cellular debris. Virions in the supernatant were sedimented through a 20% sucrose cushion (wt/wt) in TEN buffer (10 mM Tris pH 7.4, 1 mM EDTA, 100 mM NaCl) by ultracentrifugation at 25,000 rpm for 1 h at 4°C in a Beckman SW32 Ti rotor.

Pelleted MHV and TGEV virions were resuspended in MM and TEN buffer, respectively, and the infectivity was checked by using the median tissue culture infective dose ($TCID_{50}$) end-point dilution assay.

Cryo-Electron Tomography: Sample Preparation and Data Collection. Cryo-electron microscopy samples were prepared immediately after purification. Gold particles (10-nm) were added to the virus suspension to serve as fiducial markers for tomography. Drops of 5 μL of sample were applied to carbon-coated holey grids, blotted in an environmentally controlled chamber at 100% humidity, and plunged into liquid ethane.

The tilt series were collected in a 300 kV FEI Polara microscope using Xplore 3D software (FEI). The microscope was equipped with a Gatan post-column energy filter and a 2k × 2k CCD camera (Gatan). Zero-energy loss imaging was

used to collect the data. Each tilt series covered an angular range of ≈130° in 2° increments and was acquired with increasing exposure times at higher tilt angles, keeping the total dose at approximately 100 $e^{-}/Å^2$. The nominal underfocus value used was 4 μm, which ensured no contrast inversions resulting from the contrast transfer function up to approximately 3 nm. The pixel size was 0.58 nm at the specimen level.

Image Processing. Alignment and reconstruction of the tilt series were performed with TOM software Toolbox (42). The images in the tilt series were mutually aligned by using the fiducial gold markers present in the sample. A preliminary binned reconstruction of the whole field of view was calculated, and the different virions present in the sample were manually selected. Then, MHV particles were individually reconstructed by weighted back-projection to full resolution (0.58 nm voxel size). These tomograms were denoised by non-linear anisotropic diffusion (43), using the algorithm in edge enhancement mode for 20 to 30 iterations and a λ value of 0.5 SDs. An automatic procedure to ascertain both the particle centre and the envelope radius was designed and implemented in SPIDER (44). Rotationally averaged radial density profiles of the centered virions were used to determine the size and the thickness of the viral envelope (details in *SI Text* and Fig. S4). The 3D analysis and visualization of MHV envelopes was done in MATLAB (MathWorks; details in *SI Text*).

ACKNOWLEDGMENTS. We thank Heiner Friedrich, Ronald Limpens, Teresa Ruiz, Raimond Ravelli, Roman Koning, and Mieke Mommas for their assistance and advice. This work was partially supported by Marie Curie Intra-European fellowship MEIF-CT-2004–501540 (to M.B.), Dutch Organization for Scientific Research grant 813.05.001 (to B.J.B.), and VENI grant 016.062.027 (to B.J.B.).

1. Peiris JS, *et al.* (2003) Coronavirus as a possible cause of severe acute respiratory syndrome. *Lancet* 361:1319–1325.
2. Ksiazek TG, *et al.* (2003) A novel coronavirus associated with severe acute respiratory syndrome. *N Engl J Med* 348:1953–1966.
3. van der Hoek L, *et al.* (2004) Identification of a new human coronavirus. *Nat Med* 10:368–373.
4. Woo PC, *et al.* (2005) Characterization and complete genome sequence of a novel coronavirus, coronavirus HKU1, from patients with pneumonia. *J Virol* 79:884–895.
5. de Haan CA, Rottier PJ (2005) Molecular interactions in the assembly of coronavirus. *Adv Virus Res* 64:165–230.
6. Masters PS (2006) The molecular biology of coronaviruses. *Adv Virus Res* 66:193–292.
7. Vennema H, *et al.* (1996) Nucleocapsid-independent assembly of coronavirus-like particles by co-expression of viral envelope protein genes. *EMBO J* 15:2020–2028.
8. Davies HA, Dourmashkin RR, Macnaughton MR (1981) Ribonucleoprotein of avian infectious bronchitis virus. *J Gen Virol* 53:67–74.
9. Macnaughton MR, Davies HA (1978) Ribonucleoprotein-like structures from coronavirus particles. *J Gen Virol* 39:545–549.
10. Caul EO, Ashley CR, Ferguson M, Egglestone SI (1979) Preliminary studies on the isolation of coronavirus 229E nucleocapsids. *FEMS Microbiol Lett* 5:101–105.
11. Garwes DJ, Pocock DH, Pike BV (1976) Isolation of subviral components from transmissible gastroenteritis virus. *J Gen Virol* 32:283–294.
12. Risco C, Anton IM, Enjuanes L, Carrascosa JL (1996) The transmissible gastroenteritis coronavirus contains a spherical core shell consisting of M and N proteins. *J Virol* 70:4773–4777.
13. Beniac DR, Andonov A, Grudeski E, Booth TF (2006) Architecture of the SARS coronavirus prefusion spike. *Nat Struct Mol Biol* 13:751–752.
14. Neuman BW, *et al.* (2006) Supramolecular architecture of severe acute respiratory syndrome coronavirus revealed by electron cryomicroscopy. *J Virol* 80:7918–7928.
15. Baker TS, Olson NH, Fuller SD (1999) Adding the third dimension to virus life cycles: three-dimensional reconstruction of icosahedral viruses from cryo-electron micrographs. *Microbiol Mol Biol Rev* 63:862–922.
16. Mitra K, Ubarretxena-Belandia I, Taguchi T, Warren G, Engelman DM (2004) Modulation of the bilayer thickness of exocytic pathway membranes by membrane proteins rather than cholesterol. *Proc Natl Acad Sci USA* 101:4083–4088.
17. Armstrong J, Niemann H, Smeekens S, Rottier P, Warren G (1984) Sequence and topology of a model intracellular membrane protein, E1 glycoprotein, from a coronavirus. *Nature* 308:751–752.
18. Rottier P, Brandenburg D, Armstrong J, van der Zeijst B, Warren G (1984) Assembly in vitro of a spanning membrane protein of the endoplasmic reticulum: the E1 glycoprotein of coronavirus mouse hepatitis virus A59. *Proc Natl Acad Sci USA* 81:1421–1425.
19. Rottier PJ, *et al.* (1986) Predicted membrane topology of the coronavirus protein E1. *Biochemistry* 25:1335–1339.
20. Mayer T, Tamura T, Falk M, Niemann H (1988) Membrane integration and intracellular transport of the coronavirus glycoprotein E1, a class III membrane glycoprotein. *J Biol Chem* 263:14956–14963.
21. Kuo L, Masters PS (2002) Genetic evidence for a structural interaction between the carboxy termini of the membrane and nucleocapsid proteins of mouse hepatitis virus. *J Virol* 76:4987–4999.
22. Narayanan K, Chen CJ, Maeda J, Makino S (2003) Nucleocapsid-independent specific viral RNA packaging via viral envelope protein and viral RNA signal. *J Virol* 77:2922–2927.
23. Sturman LS, Holmes KV, Behnke J (1980) Isolation of coronavirus envelope glycoproteins and interaction with the viral nucleocapsid. *J Virol* 33:449–462.
24. Zhu P, *et al.* (2006) Distribution and three-dimensional structure of AIDS virus envelope spikes. *Nature* 441:847–452
25. Holmes KV, Doller EW, Sturman LS (1981) Tunicamycin resistant glycosylation of coronavirus glycoprotein: demonstration of a novel type of viral glycoprotein. *Virology* 115:334–344.
26. Rottier PJ, Horzinek MC, van der Zeijst BA (1981) Viral protein synthesis in mouse hepatitis virus strain A59-infected cells: effect of tunicamycin. *J Virol* 40:350–357.
27. Yang X, Kurteva S, Ren X, Lee S, Sodroski J (2005) Stoichiometry of envelope glycoprotein trimers in the entry of human immunodeficiency virus type 1. *J Virol* 79:12132–12147.
28. Risco C, Muntion M, Enjuanes L, Carrascosa JL (1998) Two types of virus-related particles are found during transmissible gastroenteritis virus morphogenesis. *J Virol* 72:4022–4031.
29. Salanueva IJ, Carrascosa JL, Risco C (1999) Structural maturation of the transmissible gastroenteritis coronavirus. *J Virol* 73:7952–7964.
30. Grunewald K, Cyrklaff M (2006) Structure of complex viruses and virus-infected cells by electron cryo tomography. *Curr Opin Microbiol* 9:437–442.
31. Risco C, *et al.* (1995) Membrane protein molecules of transmissible gastroenteritis coronavirus also expose the carboxy-terminal region on the external surface of the virion. *J Virol* 69:5269–5277.
32. Fujiyoshi Y, Kume NP, Sakata K, Sato SB (1994) Fine structure of influenza A virus observed by electron cryo-microscopy. *EMBO J* 13:318–326.
33. Harris A, *et al.* (2006) Influenza virus pleiomorphy characterized by cryoelectron tomography. *Proc Natl Acad Sci USA* 103:19123–19127.
34. Fuller SD, Wilk T, Gowen BE, Krausslich HG, Vogt VM (1997) Cryo-electron microscopy reveals ordered domains in the immature HIV-1 particle. *Curr Biol* 7:729–738.
35. Wilk T, *et al.* (2001) Organization of immature human immunodeficiency virus type 1. *J Virol* 75:759–771.
36. Yeager M, Wilson-Kubalek EM, Weiner SG, Brown PO, Rein A (1998) Supramolecular organization of immature and mature murine leukemia virus revealed by electron cryo-microscopy: implications for retroviral assembly mechanisms. *Proc Natl Acad Sci USA* 95:7299–7304.
37. Escors D, Ortego J, Laude H, Enjuanes L (2001) The membrane M protein carboxy terminus binds to transmissible gastroenteritis coronavirus core and contributes to core stability. *J Virol* 75:1312–1324.
38. de Haan CA, Vennema H, Rottier PJ (2000) Assembly of the coronavirus envelope: homotypic interactions between the M proteins. *J Virol* 74:4967–4978.
39. Locker JK, Opstelten DJ, Ericsson M, Horzinek MC, Rottier PJ (1995) Oligomerization of a trans-Golgi/trans-Golgi network retained protein occurs in the Golgi complex and may be part of its retention. *J Biol Chem* 270:8815–8821.
40. Opstelten DJ, Raamsman MJ, Wolfs K, Horzinek MC, Rottier PJ (1995) Envelope glycoprotein interactions in coronavirus assembly. *J Cell Biol* 131:339–349.
41. Bosch BJ, Van Der Zee R, de Haan CA, Rottier PJ (2003) The coronavirus spike protein is a class I virus fusion protein: structural and functional characterization of the fusion core complex. *J Virol* 77:8801–8811.
42. Nickell S, *et al.* (2005) TOM software toolbox: acquisition and analysis for electron tomography. *J Struct Biol* 149:227–234.
43. Frangakis AS, Hegerl R (2001) Noise reduction in electron tomographic reconstructions using nonlinear anisotropic diffusion. *J Struct Biol* 135:239–250.
44. Frank J, *et al.* (1996) SPIDER and WEB: processing and visualization of images in 3D electron microscopy and related fields. *J Struct Biol* 116:190–199.